IEEE Access
Multidisciplinary | Rapid Review | Open Access Journal

Received June 18, 2019, accepted July 12, 2019, date of publication July 16, 2019, date of current version August 6, 2019.

Digital Object Identifier 10.1109/ACCESS.2019.2929115

A Dual-Band Metasheet for Asymmetric Microwave Transmission With Polarization Conversion

SAFIULLAH KHAN, (Student Member, IEEE), AND THOMAS F. EIBERT, (Senior Member, IEEE)

Chair of High-Frequency Engineering, Department of Electrical and Computer Engineering, Technical University of Munich, 80290 Munich, Germany

Corresponding author: Safiullah Khan (safiullah.khan@tum.de)

This work was supported in part by the German Research Foundation (DFG) and in part by the Technical University of Munich (TUM) through the Open Access Publishing Program.

ABSTRACT A metamaterial-based planar polarization conversion screen is designed by exploiting the mutual interactions between two distinct types of resonators. The design starts from a unit cell comprising a subwavelength T-type resonator and a rectangular split-ring resonator (RSRR). In order to enhance the cross-polarization conversion, the unit cell is rotated by 90° to obtain a chiral geometry and the right diagonal elements are scaled down to construct a rotationally asymmetric 2×2 supercell. The supercells are arranged periodically on either side of the substrate. In the bottom layer, each element is rotated by 90° with respect to the corresponding element in the top layer to achieve the asymmetric transmission property and to introduce the desired phase difference between the two orthogonal linear vector components of the transmitted wave. The proposed design exhibits very good circular polarization efficiency, which is primarily achieved by transverse magnetic dipole–magnetic dipole coupling. The polarizer has an ellipticity of 44.4° and a polarization extinction ratio of 37.30 dB at 14.79 GHz. Furthermore, the polarization conversion ratio for both linear orthogonal components is identical at this frequency. At 9.15 GHz, strong orthogonal polarization rotation is observed. The electrical size of the unit cell is $0.25\lambda_0 \times 0.25\lambda_0 \times 0.077\lambda_0$. Simulation and measurement results are presented to verify the performance of the polarization converter.

INDEX TERMS Frequency selective surfaces, microwave propagation, polarization converter.

I. INTRODUCTION

In wireless communication systems polarization mismatch at the receiver antenna can impact the systems' propagation link budget. For example, in satellite communication a linearly polarized wave may experience rotation while propagating through the atmosphere. This effect is called Faraday rotation and it can affect the link budget [1]. Thus, a linearly polarized wave is not always suitable for transmission. Some other issues associated with linearly polarized waves are multipath fading and receiver antenna orientation. Under such circumstances, circular polarization (CP) is preferred because it shows strong immunity to environmental effects. This provides an opportunity to explore structures, which can perform linear-to-circular polarization conversion efficiently because it is not always convenient to generate CP waves at element level in planar radiating arrays. For this purpose, one solution is to use frequency selective surfaces (FSSs) as they can be used on top of the arrays.

FSSs allow waves in certain bands of frequencies to pass through and block other out-of-band frequencies or vice-versa [2]. FSSs have been extensively studied for various purposes, such as for polarization tuning, beam shaping, or gain and radar cross section improvement [3]–[7]. Parameters that determine the performance of FSSs are chosen depending on the application where they are used. For example, polarization stability, high selectivity, insertion loss, incident angle stability, band roll-off, axial ratio, and gain, etc. are some of such parameters [8]–[11]. Polarization selective surfaces (PSSs) are a type of FSSs that can convert the polarization of an incident wave in a certain band of frequencies and leave the polarization state of the out-of-band frequencies unchanged [12], [13]. It is important to understand the difference between a polarization converter and a rotator. In a polarization rotator, the out-going wave has the same polarization state as the incoming wave, but the plane of

The associate editor coordinating the review of this manuscript and approving it for publication was Lei Zhao.

polarization is rotated by a certain angle for the out-going wave. In a polarization converter, the polarization state of the out-going wave is changed, i.e., linear polarization (LP) to CP. Using polarization converters on top of an LP antenna allows to separate the antenna array design and the creation of CP waves.

Polarization conversion occurs because of a phase difference between the orthogonal components of a reflected or a transmitted wave. The phase difference can be artificially achieved in different ways: 1) by using an anisotropic chiral structure geometry [14], whose no-mirror symmetry ensures the twisting response [15], i.e., 2D Archimedes spiral or 3D helix; 2) by using a cascaded capacitive impedance layer and an inductive impedance layer, both having a different response for the two orthogonal components of an incident electromagnetic (EM) wave [16], leading to a phase difference of 90° after tuning; and 3) by using an active metasurface, which has embedded varactor diodes to impose a phase difference between the orthogonal components of the incident plane wave [5].

A comparative study of various designs of flexible chiral metamaterials (MTMs) for the terahertz regime was presented in [17]. Chiral properties, such as optical activity (polarization rotation of the LP waves), circular polarization generation, circular dichroism (the absorption difference between right- and left-handed circularly polarized waves) and filtering capabilities for the designs were compared. Large optical activity in all the designs was observed, but the ellipticity remained below 35°. In [12], a tri-layered metasurface was proposed to achieve polarization rotation. The metallic gratings on each layer were successively rotated by 0°, 45°, and 90° to demonstrate rotation of the incident linearly x-polarized wave to the transmitted linearly y-polarized wave. Recently, polarization converters based on triple twisted SRRs, substrate integrated waveguides, and miniaturized-element FSSs have been proposed [16], [19], [20]. Most of the work has been focused around single-band polarization conversion. Multilayered structures have been used where an increase in the bandwidth or multi-band operation was reported [21], [22]. A better and wider axial ratio could also be achieved. However, this approach introduces higher insertion loss (IL) and may increase the return loss (RL) due to poor matching. Multilayered structures also require careful fabrication and alignment. The quantities IL and RL are important factors while designing structures for radar applications and satellite communication [23]. For example, in an imaging system, poor matching will damage the quality of the image due to multiple interactions within the system [9].

In this paper, a double layer MTM unit cell structure, which is composed of two distinct types of resonators is proposed as a polarization converter. The characteristics of corresponding single layer designs were previously explored as an FSS for waveguide filter and microwave absorption applications in [24]. An application as an energy harvester was studied in [25], [26]. In this work, the structure is re-designed by introducing geometric asymmetries. The multiple resonators based design is used to exploit the mutual coupling of the structure to achieve a strong cross-polarized microwave transmission and a highly-selective polarization conversion. The design is investigated with respect to the following features: 1) The mutual interaction between the two distinct resonators in a unit cell and other resonators in the array configuration provides freedom to control the resonance frequency and the ellipticity with very few parameters. 2) In dual band behavior, when a linearly polarized wave is incident on the metasheet a strong cross-polarized transmitted wave is obtained in one band and a circularly polarized transmitted wave is created in the other band with high polarization conversion efficiency.

In Section II, the basic principles and analytical expressions associated with the design are discussed. In Section III, the geometry and parameters of the proposed design are presented. The results are discussed and compared with some recent designs from the literature in Section IV followed by the conclusion in Section V.

II. PRINCIPLES AND FUNDAMENTAL THEORY

MTM based PSSs are composed of subwave length resonating elements to form a unit cell. The unit cells are arranged periodically to form a metasheet. The mutual coupling among the resonating elements in the metasheet, if controlled, allow to achieve the desired electromagnetic characteristics. The proposed design uses an anisotropic structure and the constitutive relations are given by [18]

$$\mathbf{D} = \epsilon_\circ \epsilon_r \mathbf{E} - \frac{j\kappa}{c_\circ}\mathbf{H}, \tag{1}$$

$$\mathbf{B} = \mu_\circ \mu_r \mathbf{H} + \frac{j\kappa}{c_\circ}\mathbf{E}, \tag{2}$$

where κ describes the strength of cross-coupling between magnetic and electric field and is known as *chirality*. $\epsilon_\circ$ (ϵ_r) and $\mu_\circ$ (μ_r) represent free-space (relative) permittivity and permeability, respectively. The speed of light in free-space is denoted by $c_\circ$. When a linearly polarized wave is incident on such a structure then the circularly polarized transmitted waves are given as

$$\mathbf{E}^{\pm}(z) = \frac{1}{2}E_\circ(\hat{x} \mp j\hat{y})e^{-jkz}, \tag{3}$$

where $\mathbf{E}^+$ and $\mathbf{E}^-$ represent the right hand circularly polarized (RHCP) wave and the left hand circularly polarized (LHCP) wave, respectively. The time dependence $e^{j\omega t}$ is suppressed. In the above expression, the direction of propagation is in $+z$-direction and the index of refraction for such a wave is given by $n_\pm = n \pm \kappa$. Consider a y-polarized incident wave (E_y^i) which propagates through this structure. The transmitted wave will have two orthogonal linear components, T_{yy} and T_{xy} (where the first subscript and the second subscript indicate the polarization of the transmitted wave and the incident wave, respectively). The transmission coefficients for CP waves can be obtained from linear transmission coefficients as

$T^{\pm} = 1/\sqrt{2}(T_{yy} \pm jT_{xy})$. The performance of the polarization converter can be evaluated by the ellipticity η (it measures the circular dichroism and characterizes the polarization state of the transmitted wave), the polarization extinction ratio PER (it measures the difference between the magnitude of the RHCP and the LHCP waves) [19], and the polarization conversion ratio PCR (it measures the polarization conversion of an LP incident wave to the transmitted cross- and co-component),

$$\eta = \arctan\left(\frac{|T^+| - |T^-|}{|T^+| + |T^-|}\right) = 0.5 \arcsin\left(\frac{|T^+|^2 - |T^-|^2}{|T^+|^2 + |T^-|^2}\right), \quad (4)$$

$$\text{PER} = 20 \log_{10}(|T_{+x(y)}|/|T_{-x(y)}|), \quad (5)$$

$$\text{PCR}_{yy} = |T_{yy}|^2/(|T_{yy}|^2 + |T_{xy}|^2), \quad (6)$$

$$\text{PCR}_{xy} = |T_{xy}|^2/(|T_{yy}|^2 + |T_{xy}|^2). \quad (7)$$

The wave is circularly polarized when $\eta = \pm 45°$, linearly polarized when $\eta = 0°$, and for all other values of η the wave is elliptically polarized. Large values of PER mean high polarization conversion efficiency.

High polarization conversion efficiency is achieved when either $|T^+|$ or $|T^-|$ is zero. This means that the magnitude of the transmitted wave components $|T_{yy}|$ ($|T_{xx}|$) and $|T_{xy}|$ ($|T_{yx}|$) must be equal and their phase difference should be $-90°$ or $90°$ for a RHCP or a LHCP wave, respectively.

III. POLARIZER DESIGN

The unit cell of the proposed design consists of two distinct metamaterial resonators, a rectangular split ring resonator (RSRR) and a T-type resonator. First, the unit cell is rotated by 90° clockwise to create a C4 symmetric 2 × 2 supercell. Each unit cell of the super cell in the bottom layer is rotated by 90° with respect to the corresponding unit cell in the top layer. The structure now forms a chiral geometry and it is three dimensional nonsymmetric. It is pertinent to mention here that the chirality only affects the polarization state of the propagating wave [18]. Chiral geometries obey fixed relations for certain symmetries. For example, the LP transmission coefficients for the C4 symmetric structures are $T_{xx}^{f(b)} = T_{yy}^{f(b)}$ and $T_{yx}^{f(b)} = -T_{xy}^{f(b)}$ (where the superscript f represents a wave propagating in $-z$-direction and the superscript b represents a wave propagating in z-direction) when the incident wave is LP. Second, the right diagonal resonating elements in the supercell are scaled 0.5 times the left diagonal resonating elements (all the parameters are scaled except w, which is the same for all the elements) as shown in Fig. 1(a). The structure is designed as C4 nonsymmetric in order to increase the cross-polarization conversion. As a result, the LP transmission coefficients for the C4 nonsymmetric structures become $T_{xx}^{f(b)} = T_{yy}^{f(b)}$ and $T_{yx}^{f(b)} \neq T_{xy}^{f(b)} = T_{xy}^{b(f)}$. Since each layer responds differently to orthogonal components of the incident electric field, the desired phase difference can be achieved. The interlayer coupling is affected by the thickness of the dielectric substrate. If the thickness is zero, the missing symmetry in z-direction will vanish resulting in no chirality and when the thickness is too large coupling will be too weak.

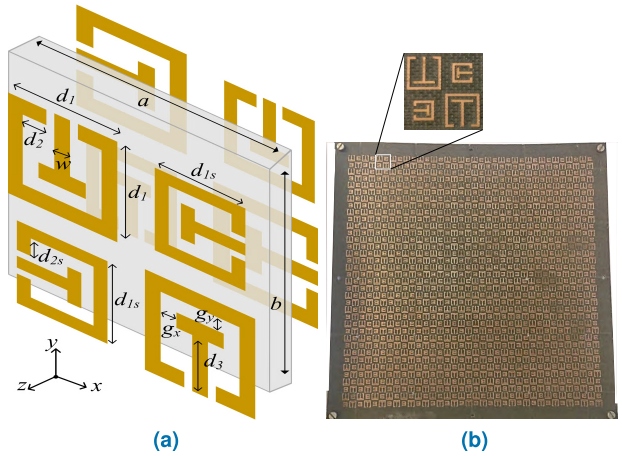

FIGURE 1. Polarization selective surface (a) Proposed supercell where $a = b = 10$ mm, $d_1 = 4.5$ mm, $d_2 = 0.75$ mm, $d_3 = 3.3$ mm, $d_{1s} = 0.5 \times d_1 = 2.7$ mm, $d_{2s} = 0.5 \times d_2 = 0.375$ mm, $w = 0.4$ mm, and $g_x = g_y = 0.4$ mm (b) Fabricated sheet.

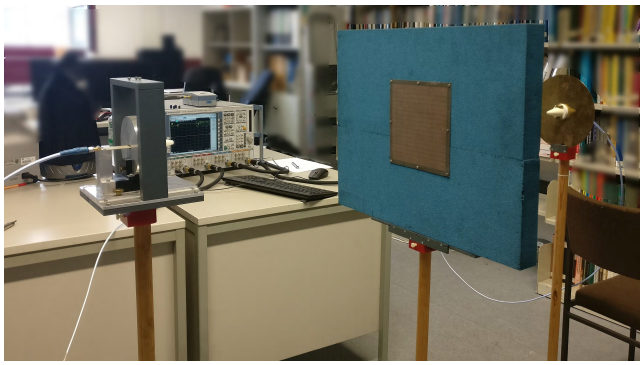

FIGURE 2. Polarization selective surface free-space measurement setup.

The dielectric substrate used in the proposed design is Rogers DiClad 880 with a relative permittivity $\epsilon_r = 2.2$, a loss tangent of 0.0009 (from datasheet) and a thickness of 1.524 mm. Fig. 1(b) shows the fabricated sample. The fabricated sheet consists of 18 × 18 supercells. The average size of the unit cell is $\lambda_r/4$ and of the supercell is $\lambda_r/2$ (λ_r corresponds to the resonance frequency 14.79 GHz). The proposed structure was designed in CST Microwave Studio with periodic boundary conditions in (x, y)-direction and Floquet ports in z-direction [28].

IV. RESULTS AND DISCUSSION

A linearly polarized plane wave is incident on the structure and the orthogonal linear vector components of the transmitted wave are computed on the other side of the structure to study the propagation behavior. For the purpose of measurements, the free-space setup shown in Fig. 2 was used. The transmission measurements were performed using two linearly polarized dipole excited ultrawideband dielectric rod antennas with a reflector. The input reflection of the antennas remains below −10 dB from 3 GHz up to 20 GHz. The details

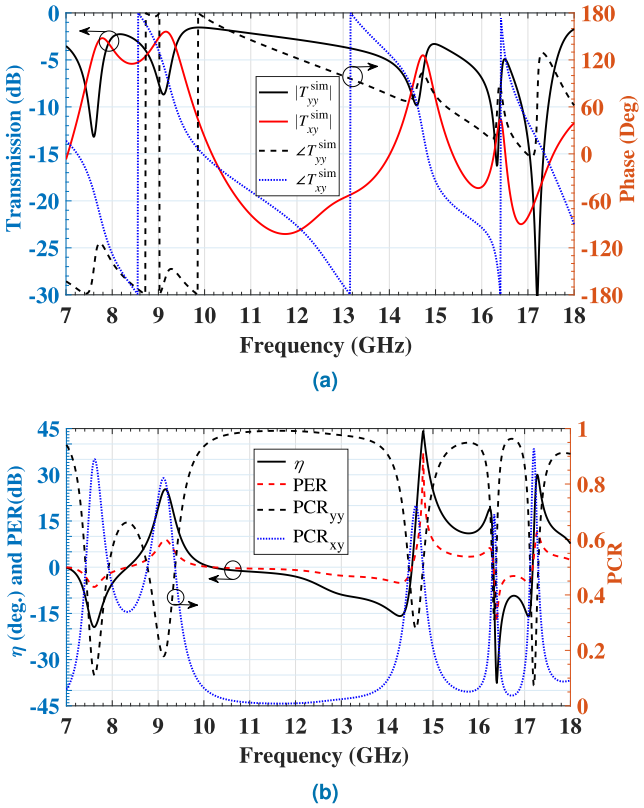

FIGURE 3. (a) Magnitude and phase of cross- and co- components of the transmission coefficient. (b) Simulated performance indicators for PSS.

of the antennas can be found in [29]. The polarization state of the antenna is changed by physically rotating the antenna orientation on the transmission side of the metasheet.

The transmission coefficients for $E_y^i(-z)$ at normal incidence as a function of frequency are shown in Fig. 3(a). The first and second null of the co-component of the transmission coefficient magnitude ($|T_{yy}|$), represented by the black through line, occur at 7.6 GHz and 9.15 GHz, respectively. These resonances are the combined effect (resonance and mutual interactions) of the left diagonal elements on both layers. The resonance at 14.6 GHz is predominantly due to the combined effect of the right diagonal elements on both layers. Consequently, a strong cross-component (red through line) of the transmission coefficient ($|T_{xy}|$) is observed at these frequencies. It is further seen that the magnitudes of both components are identical at 14.79 GHz. The difference between the phases of orthogonal components determines the polarization type of the transmitted wave. The phase of co-component and cross-component at 14.79 GHz is 97.78° and 8.39°, respectively, yielding a phase difference of $\Delta\phi = \angle T_{xy} - \angle T_{yy} = -89.39°$. Thus, a circular polarized wave is created on the transmission side of the PSS at 14.79 GHz and a strong cross-component with a magnitude as high as −2 dB at 9.15 GHz. In Fig. 3(b), the performance parameters defined in eqs. (4) - (7) are plotted. It can be seen that the peak value of the ellipticity η is 44.3° at 14.79 GHz, which means that the transmitted wave is circularly polarized at this frequency. Furthermore, the value of η at 9.15 GHz is 25.2° which represents the elliptical polarization. Other peak values of η correspond to transmission magnitudes lower than −10 dB, hence they are not considered. An additional functionality of the proposed PSS is demonstrated by the PER and PCR. The PER shows that the magnitude of the RHCP wave is greater than the LHCP wave at 9.15 GHz and 14.79 GHz by a margin of 8.83 dB and 37.30 dB, respectively. This implies that the transmitted wave is RHCP (with respect to the $-z$-direction) at 14.79 GHz. The magnitude of the orthogonal components that constitute the RHCP wave show the PSS conversion efficiency. It can be observed that the structure polarization conversion ratio PCR is 0.5 for $|T_{yy}|$ and $|T_{xy}|$ at 14.79 GHz. Fig. 3(b) also shows that the transmitted wave has a $y-$polarized dominant component between 10 GHz to 13 GHz.

The polarization conversion behavior of the proposed structure can be understood by analyzing the fields and the surface current distributions. At resonances, high cross-polarization transmission or polarization conversion are the consequence of longitudinal dipole-dipole coupling and transverse (interlayer) coupling. The superposition of the modes produced due to magnetic dipoles and electric dipoles can be expressed by eigenmodes of the resonator. Fig. 4 illustrates the surface current plot over the $z-$component of the electric field at different resonance frequencies. At 14.79 GHz, in the top layer, a longitudinal electric dipole mode is observed in each of the two RSRR elements on the left diagonal with weak coupling within the supercell and strong coupling with the elements in the neighboring supercells. A magnetic dipole mode is observed in the right diagonal elements due to the small size of the elements and alignment of the gaps along the incident electric field vector ($y-$axis). The loop current and charge distribution (strong E_z on the T-type resonator) can been seen in Fig. 4(a). In addition, coupling due to parallel and antiparallel currents within the unit cell can be interpreted accordingly. The bottom layer for this frequency is shown in Fig. 4(b). The currents for the left diagonal elements are reversed. In the case of the right diagonal elements, the currents in the outer loop remain the same on the top layer and on the bottom layer, which indicates parallel magnetic dipole coupling. The direction of the currents on the bottom layer distinguishes the rotation direction and determines the RHCP or the LHCP type of the transmitted wave. The parallel currents on both layers at 14.79 GHz indicate that the transmitted wave is RHCP. At 16.4 GHz, the currents on the top layer are almost the same as for 14.79 GHz, especially, on the right diagonal elements, as shown in Fig. 4(c). Fig. 4(d) shows that the currents are antiparallel (opposite in direction) on the right diagonal elements of the bottom layer with respect to the top layer, resulting in a LHCP wave. The lateral coupling in the gaps between an RSRR and a T-type resonator within the unit cell affects the resonance frequency (the parameters (g_x, d_2), as shown in Fig. 1(a), can be used to change the gap size). The advantage of using different types of resonators

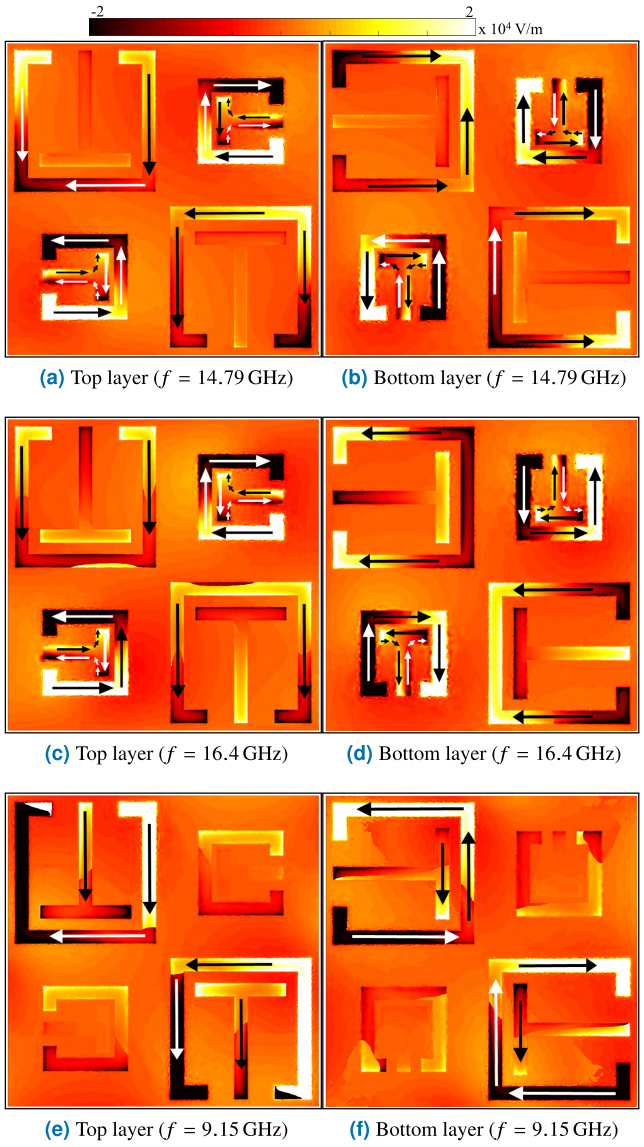

FIGURE 4. Symbolic electric surface current distribution (black or white arrows) over electric field component E_z (color scale), which is related to surface charge, at different frequencies.

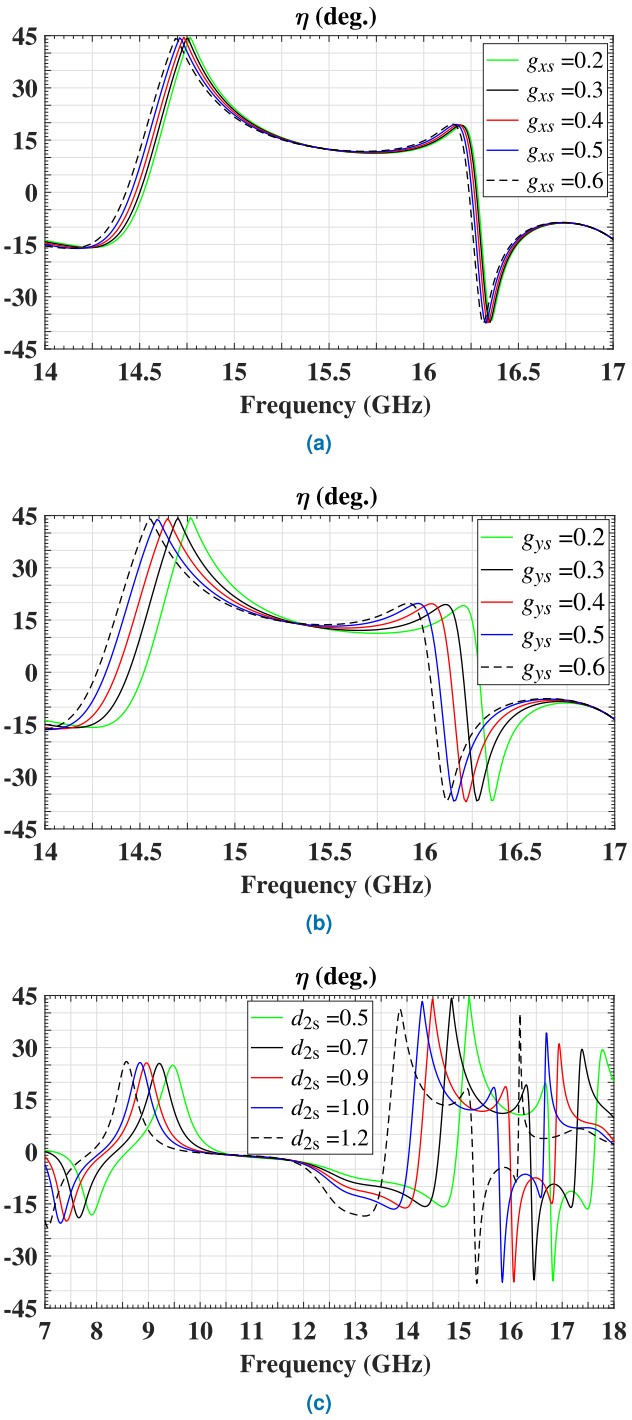

FIGURE 5. Effect of parameters on the transmission behavior and the resonance frequencies. Ellipticity as a function of frequency when only (a) g_{xs} is varied, (b) g_{ys} is varied, and (c) d_2 is varied in millimeters.

in a unit cell is that there are multiple regions where strong coupling can be observed. These regions give the flexibility to control the electromagnetic behavior of the structure. In the particular design those regions are represented by g_x, g_y, and the gap between the RSRR and the T-type resonator at the top. At 9.15 GHz, strong cross-polarization conversion is observed. Field distributions inside the structure are twisted as a result of the antiparallel current flow as shown in Fig. 4(e) and Fig. 4(f).

It is clear that in resonant structures the incident electromagnetic wave causes strong electric fields in the gaps and strong magnetic fields around the electric currents in metallic strips. This interaction between metasheet and electromagnetic wave along with the mutual coupling between the resonators within the unit cell is responsible for the overall behavior of the FSS. Therefore, the two controlling factors are the geometry of the elements in a unit cell and the spacing between the elements. A multi-resonators based approach is used to create small capacitive gaps within a unit cell, which can provide tunability by changing the coupling between the elements. In particular, a T-type resonator was chosen because it is center connected, behaves like an electric dipole for parallel electric field incidence, and it does not

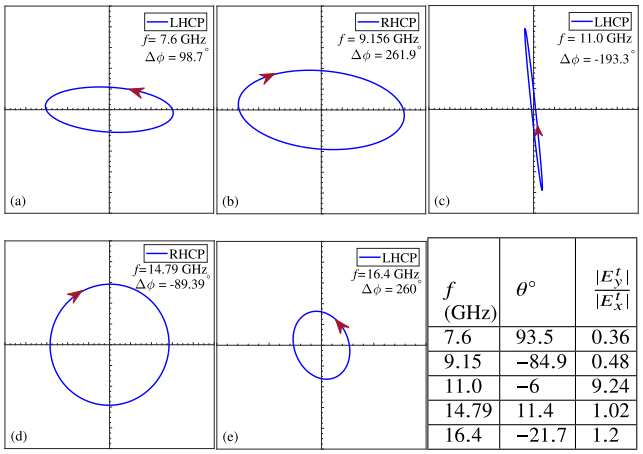

f (GHz)	$\theta°$	$\frac{\lvert E_y^t\rvert}{\lvert E_x^t\rvert}$
7.6	93.5	0.36
9.15	−84.9	0.48
11.0	−6	9.24
14.79	11.4	1.02
16.4	−21.7	1.2

FIGURE 6. Electric field trace of the transmission coefficient when the incident wave is LP. The arrow indicates the direction of rotation in time. The major axis makes (a) 93.5° (b) −84.9° (c) −6° (d) 11.4° (e) −21.7° with respect to the y-axis. Positive and negative sign of θ represent the clockwise and the counter-clockwise sense of polarization azimuth angle rotation, respectively.

affect the inter-element spacing in an array formed by the RSRRs. At its edges/corners, the T-type structure establishes three regions of strong coupling (g_x, g_y, and the gap at the top of the unit cell) with the RSRR, which allows to control the resonance frequency with very few parameters. This is demonstrated in Fig. 5. In Fig. 5(a), g_{xs} represents the lateral gaps between the RSRR and the T-type resonator at the bottom of the unit cells located on the right diagonal in a supercell. As seen from the electric surface current distribution, the right diagonal elements predominantly contribute to the second resonance and produce an RHCP wave. When g_{xs} is changed from 0.2 mm to 0.6 mm, the resonance frequency shifts to lower frequencies. The tunable bandwidth is 88 MHz for only 0.5 mm change and the ellipticity remains at above 44°. The lower resonance frequency remains unchanged and is hence not shown. Similarly, g_{ys} represents the vertical gap between the RSRR and the T-type resonator for the right diagonal elements. In Fig. 5(b), it can be seen that when g_{ys} changes from 0.2 mm to 0.6 mm the resonance frequency shifts to lower values. The tunable bandwidth in this range is 230 MHz where the ellipticity is above 44°. Fig. 5(c) shows the effect on both resonance frequencies when d_{2s} is changed. Increasing d_{2s}, shifts the resonance frequency to lower values and does not affect the ellipticity significantly. The tunable bandwidth is 1.35 GHz when d_{2s} changes from 0.5 mm to 1.2 mm. In resonant structures, the effective permittivity and permeability change very sharply around the resonance frequency. This means that a small change in the frequency results in a significant change in permittivity and permeability (this concept is often exploited in sensors).

The polarization states of the transmitted wave for a $y-$polarized incident wave are illustrated in Fig. 6. In general the transmitted waves have elliptical polarization except at the resonance frequency, where the transmitted wave is circular polarized. When the major axis of the ellipse rotates with respect to the polarization of the incident wave, the angle of

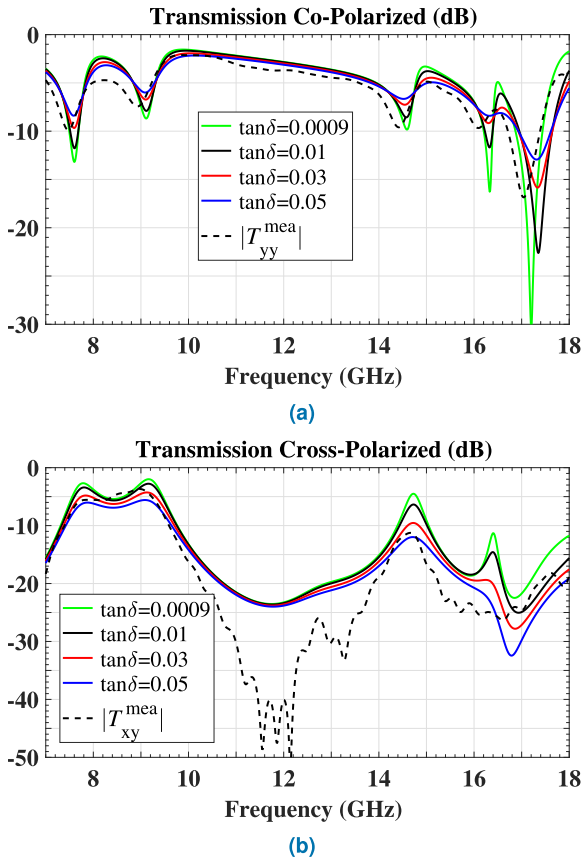

FIGURE 7. Transmitted orthogonal components obtained with measurement setup shown in Fig. 2.

rotation is called polarization azimuth angle and it is defined as, $\theta = [arg(T^+) - arg(T^-)]/2$. Due to a strong cross polarized component, the transmitted wave is elliptical at low frequencies as shown in Fig. 6(a) and 6(b). The weak cross polarized component between 10 GHz and 13 GHz results in a very thin ellipse as depicted in Fig. 6(c). Additionally, small rotation is observed in this region. Strong resonance and mutual interactions at 14.79 GHz and 16.4 GHz in both layers cause the $n\pi/2$ phase difference and equal magnitudes, hence the RHCP and the LHCP waves are created as shown in Fig. 6(d) and 6(e). The table in Fig. 6 shows the polarization azimuth angle in degrees and the ratio between the amplitudes of the orthogonal components of the transmitted wave for the corresponding frequencies.

The simulated PSS was realized for an experimental demonstration. The results are shown in Fig. 7. The resonance frequencies from the simulation and the measurement are in good agreement but a decline in magnitude was observed in the measurements particularly for the co-polarized component. Also, it is observed that the material loss effects the resonances differently at low frequencies than at high frequencies. This magnitude reduction is caused by the losses of the substrate. It is known that the performance of the polarization converter is greatly affected by slight changes in the dielectric losses [15]. Therefore, a comparison is shown for better understanding of the behavior.

TABLE 1. Performance comparison of different polarization converters.

Ref.	Thickness (λ_0)	PER (dB)	η (deg.)	No. of layers
[19]	0.027	26.1	42.17°	3
[16]	0.18	N/A	N/A	6
[30]	0.036	N/A	~ 36.0°	2
[31]	0.024	< 10	~ 24.4°*	2
[32]	0.034	21.1	~ 41.0°	2
[33]	0.035*1	~ 37.0*2 & ~ 24.0*3	N/A	2
[34]	0.053	N/A	N/A	3
[35]	0.176	< 12	N/A	3D
present work	0.035*1 & λ_r = 0.077	37.3	44.4°	2

* for the values of $t_{+y} = -3.5$ dB and $t_{-y} = -12.0$ dB taken from Fig. 3(b)

*1 at 7.0 GHz, *2 taken from Fig. 5(a), *3 taken from Fig. 7(a)

In Table 1, a comparison with some previously presented designs is made based on the key performance parameters. The proposed design shows improvement in ellipticity and PER, but has a larger thickness compared to some of the references mentioned (due to the available fabrication facility a thinner substrate could not be used). However, the thickness can be further reduced by using a suitable substrate. In [33], the thickness of the unit cell is the same as in the presented design but the period of the unit cell is 13 mm while the period of the presented unit cell is 5 mm and the supercell is 10 mm.

V. CONCLUSION

An asymmetric polarization selective surface design based on metamaterial resonators of different kind has been proposed. Strong cross polarization rotation and conversion has been observed, which is as high as −2 dB and −4.5 dB at 9.15 GHz and 14.79 GHz, respectively. The surface current distribution and surface charges are used to illustrate the twisting and coupling effects. This further helps in distinguishing the RHCP and the LHCP waves. The results were validated experimentally. The design offers miniaturization, excellent polarization conversion efficiency, tunability, and resonance control.

REFERENCES

[1] D. M. L. Vine and S. Abraham, "The effect of the ionosphere on remote sensing of sea surface salinity from space: Absorption and emission at L band," *IEEE Trans. Geosci. Remote Sens.*, vol. 40, no. 4, pp. 771–782, Apr. 2002.

[2] B. A. Munk, *Frequency Selective Surfaces: Theory and Design*. Hoboken, NJ, USA: Wiley, 2005.

[3] Q. Guo, Z. Li, J. Su, J. Song, and L. Y. Yang, "Active frequency selective surface with wide reconfigurable passband," *IEEE Access*, vol. 7, pp. 38348–38355, Mar. 2019.

[4] M. Akbari, S. Gupta, M. Farahani, A. R. Sebak, and T. A. Denidni, "Gain enhancement of circularly polarized dielectric resonator antenna based on FSS superstrate for MMW applications," *IEEE Trans. Antennas Propag.*, vol. 64, no. 12, pp. 5542–5546, Dec. 2016.

[5] X. Gao, W. L. Yang, H. F. Ma, Q. Cheng, X. H. Yu, and T. J. Cui, "A reconfigurable broadband polarization converter based on an active metasurface," *IEEE Trans. Antennas Propag.*, vol. 66, no. 11, pp. 6086–6095, Nov. 2018.

[6] C. Chen, Z. Li, L. Liu, J. Xu, P. Ning, B. Xu, X. Chen, and C. Q. Gu, "A circularly-polarized metasurfaced dipole antenna with wide axial-ratio beamwidth and RCS reduction functions," *Prog. Electromagn. Res.*, vol. 154, pp. 79–85, Dec. 2015.

[7] H. Li, B.-Z. Wang, G. Zheng, W. Shao, and L. Guo, "A reflectarray antenna backed on FSS for low RCS and high radiation performances," *Prog. Electromagn. Res. C*, vol. 15, pp. 145–155, Aug. 2010.

[8] H. B. Wang and Y. J. Cheng, "Frequency selective surface with miniaturized elements based on quarter-mode substrate integrated waveguide cavity with two poles," *IEEE Trans. Antennas Propag.*, vol. 64, no. 3, pp. 914–922, Mar. 2016.

[9] C. Dietlein, A. Luukanen, Z. Popović, and E. Grossman, "A W-band polarization converter and isolator," *IEEE Trans. Antennas Propag.*, vol. 55, no. 6, pp. 1804–1809, Jun. 2007.

[10] X.-C. Zhu, W. Hong, K. Wu, H.-J. Tang, Z.-C. Hao, J.-X. Chen, H.-X. Zhou, and H. Zhou, "Design of a bandwidth-enhanced polarization rotating frequency selective surface," *IEEE Trans. Antennas Propag.*, vol. 62, no. 2, pp. 940–944, Feb. 2014.

[11] M. Euler, V. Fusco, R. Cahill, and R. Dickie, "Comparison of frequency-selective screen-based linear to circular split-ring polarisation convertors," *IET Microw., Antennas Propag.*, vol. 4, no. 11, pp. 1764–1772, Nov. 2010.

[12] L. Cong, W. Cao, X. Zhang, Z. Tian, J. Gu, R. Singh, J. Han, and W. Zhang, "A perfect metamaterial polarization rotator," *Appl. Phys. Lett.*, vol. 103, Oct. 2013, Art. no. 171107.

[13] H.-P. Li, G.-M. Wang, J.-G. Liang, and X.-J. Gao, "Wideband multifunctional metasurface for polarization conversion and gain enhancement," *Prog. Electromagn. Res.*, vol. 155, pp. 115–125, 2016.

[14] V. A. Fedotov, P. L. Mladyonov, S. L. Prosvirnin, A. V. Rogacheva, Y. Chen, and N. I. Zheludev, "Asymmetric propagation of electromagnetic waves through a planar chiral structure," *Phys. Rev. Lett.*, vol. 97, Oct. 2006, Art. no. 167401.

[15] O. Fernández, A. Gómez, J. Basterrechea, and A. Vegas, "Reciprocal circular polarization handedness conversion using chiral metamaterials," *IEEE Antennas Wireless Propag. Lett.*, vol. 16, pp. 2307–2310, Jun. 2017.

[16] S. M. A. M. H. Abadi and N. Behdad, "Wideband linear-to-circular polarization converters based on miniaturized-element frequency selective surfaces," *IEEE Trans. Antennas Propag.*, vol. 64, no. 2, pp. 525–534, Feb. 2016.

[17] G. Kenanakis, R. Zhao, A. Stavrinidis, G. Konstantinidis, N. Katsarakis, M. Kafesaki, C. M. Soukoulis, and E. N. Economou, "Flexible chiral metamaterials in the terahertz regime: A comparative study of various designs," *Opt. Mater. Express*, vol. 2, no. 12, pp. 1702–1712, Nov. 2012.

[18] I. V. Lindell, A. H. Sihvola, S. A. Tretyakov, and A. J. Viitanen, *Electromagnetic Waves in Chiral and Bi-Isotropic Media*. Norwood, MA, USA: Artech House, 1994, pp. 13–36.

[19] Y. Cheng, C. Wu, Z. Z. Cheng, and R. Z. Gong, "Ultra-compact multi-band chiral metamaterial circular polarizer based on triple twisted split-ring resonator," *Prog. Electromagn. Res.*, vol. 155, pp. 105–113, Mar. 2016.

[20] M. S. J. Moghadam, M. Akbari, F. Samadi, and A.-R. Sebak, "Wideband cross polarization rotation based on reflective anisotropic surfaces," *IEEE Access*, vol. 6, pp. 15919–15925, Mar. 2018.

[21] Y. Zhang, J. Zhu, C. Huang, and S. Ma, "Wide-band and high-efficiency 90° polarization rotator based on tri-layered perforated metal films," *J. Lightw. Technol.*, vol. 35, no. 21, pp. 4817–4823, Nov. 1, 2017.

[22] X. Liu, J. Zhang, W. Li, R. Lu, L. Li, Z. Xu, and A. Zhang, "Three-band polarization converter based on reflective metasurface," *IEEE Antennas Wireless Propag. Lett.*, vol. 16, pp. 924–927, Apr. 2017.

[23] M. Hosseini and S. V. Hum, "A circuit-driven design methodology for a circular polarizer based on modified Jerusalem cross grids," *IEEE Trans. Antennas Propag.*, vol. 65, no. 10, pp. 5322–5331, Oct. 2017.

[24] S. Khan and T. F. Eibert, "A multifunctional metamaterial-based dual-band isotropic frequency-selective surface," *IEEE Trans. Antennas Propag.*, vol. 66, no. 8, pp. 4042–4051, Aug. 2018.

[25] S. Khan and T. F. Eibert, "A highly efficient miniaturized microwave collector for wireless power transmission," in *Proc. Appl. Comput. Electromagn. Soc. Symp. (ACES)*, Denver, CO, USA, 2018, pp. 1–2.

[26] S. Khan and T. F. Eibert, "A multi-resonant meta-absorber as an electromagnetic energy harvester," in *Proc. IEEE Int. Symp. Antennas Propag. (APSURSI)*, San Diego, CA, USA, Jul. 2017, pp. 1091–1092.

[27] R. Zhao, T. Koschny, and C. M. Soukoulis, "Chiral metamaterials: Retrieval of the effective parameters with and without substrate," *Opt. Express*, vol. 18, no. 14, pp. 14553–14567, Jul. 2010.
[28] Microwave Studio, Darmstadt, Germany. (2016). *CST Computer Simulation Technology*. [Online]. Available: https://www.cst.com
[29] M. D. Blech and T. F. Eibert, "A dipole excited ultrawideband dielectric rod antenna with reflector," *IEEE Trans. Antennas Propag.*, vol. 55, no. 7, pp. 1948–1954, Jul. 2007.
[30] M. L. N. Chen, L. J. Jiang, W. E. I. Sha, W. C. H. Choy, and T. Itoh, "Polarization control by using anisotropic 3-D chiral structures," *IEEE Trans. Antennas Propag.*, vol. 64, no. 11, pp. 4687–4694, Nov. 2016.
[31] L. Wu, Z. Yang, Y. Cheng, R. Gong, M. Zhao, Y. Zheng, J. Duan, and X. Yuan, "Circular polarization converters based on bi-layered asymmetrical split ring metamaterials," *Appl. Phys. A, Solids Surf.*, vol. 116, no. 2, pp. 643–648, Feb. 2014.
[32] Y. Cheng, Y. Nie, Z. Cheng, and R. Z. Gong, "Dual-band circular polarizer and linear polarization transformer based on twisted split-ring structure asymmetric chiral metamaterial," *Prog. Electromagn. Res.*, vol. 145, pp. 263–272, Apr. 2014.
[33] Y. Zhao, A. Qing, Y. Meng, Z. Song, and C. Lin, "Dual-band circular polarizer based on simultaneous anisotropy and chirality in planar metamaterial," *Sci. Rep.*, vol. 8, no. 1729, Jan. 2018.
[34] R. Zhao, H.-Y. Chen, L. Zhang, F. Li, P. Zhou, J. Xie, and L.-J. Deng, "Design and implementation of high efficiency and broadband transmission-type polarization converter based on diagonal split-ring resonator," *Prog. Electromagn. Res.*, vol. 161, pp. 1–10, Feb. 2018.
[35] S. Wu, S. Xu, T. L. Zinenko, V. V. Yachin, S. L. Prosvirnin, and V. R. Tuz, "3D-printed chiral metasurface as a dichroic dual-band polarization converter," *Opt. Lett.*, vol. 44, no. 4, pp. 1056–1059, Jan. 2019.

SAFIULLAH KHAN (S'17) received the B.S. degree in telecommunication engineering from the National University of Computer and Emerging Sciences, Islamabad, Pakistan, in 2011, and the M.S. degree in electronic engineering from the Ghulam Ishaq Khan (GIK) Institute, Topi, Pakistan, in 2014. He is currently pursuing the Dr.-Ing. (Ph.D.) degree with the Chair of High-Frequency Engineering, Department of Electrical and Computer Engineering, Technical University of Munich, Munich, Germany. From 2014 to 2015, he was Research Associate with the Faculty of Engineering Sciences, GIK Institute. His current research interests include wave propagation in complex media, frequency selective surfaces, microwave filters, antenna design, and electromagnetic energy harvesting.

THOMAS F. EIBERT (S'93–M'97–SM'09) received the Dipl.-Ing. (FH) degree from Fachhochschule Nürnberg, Nuremberg, Germany, in 1989, the Dipl.-Ing. degree from Ruhr-Universität Bochum, Bochum, Germany, in 1992, and the Dr.-Ing. degree from Bergische Universität Wuppertal, Wuppertal, Germany, in 1997, all in electrical engineering. From 1997 to 1998, he was with the Radiation Laboratory, Electrical Engineering and Computer Science Department, University of Michigan, Ann Arbor, MI, USA; from 1998 to 2002, he was with Deutsche Telekom, Darmstadt, Germany; and from 2002 to 2005, he was with the Institute for High-Frequency Physics and Radar Techniques, FGAN e.V., Wachtberg, Germany, where he was the Head of the Department Antennas and Scattering. From 2005 to 2008, he was a Professor of radio frequency technology with Universität Stuttgart, Stuttgart, Germany. Since 2008, he has been a Professor of high-frequency engineering with the Technical University of Munich, Munich, Germany. His major research interests include numerical electromagnetics, wave propagation, measurement and field transformation techniques for antennas and scattering, as well as all kinds of antenna and microwave circuit technologies for sensors and communications.